

## Effects of $\gamma$ -ray radiation on two-dimensional molybdenum disulfide ( $\text{MoS}_2$ ) nanomechanical resonators

Jaesung Lee,<sup>1,a)</sup> Matthew J. Krupcale,<sup>1,2,a)</sup> and Philip X.-L. Feng<sup>1,b)</sup>

<sup>1</sup>Department of Electrical Engineering and Computer Science, Case School of Engineering, Case Western Reserve University, 10900 Euclid Avenue, Cleveland, Ohio 44106, USA

<sup>2</sup>Department of Physics, College of Arts and Sciences, Case Western Reserve University, 10900 Euclid Avenue, Cleveland, Ohio 44106, USA

(Received 1 November 2015; accepted 26 December 2015; published online 13 January 2016)

We report on experimental investigation and analysis of  $\gamma$ -ray radiation effects on two-dimensional molybdenum disulfide ( $\text{MoS}_2$ ) drumhead nanomechanical resonators vibrating at megahertz frequencies. Given calibrated dosages of  $\gamma$ -ray radiation of  $\sim 5000$  photons with energy at 662 keV, upon exposure over 24 or 12 h, all the  $\text{MoS}_2$  resonators exhibit  $\sim 0.5$ – $2.1\%$  resonance frequency upshifts due to the ionizing  $\gamma$ -ray induced charges and their interactions. The devices show  $\gamma$ -ray photon responsivity of  $\sim 30$ – $82$  Hz/photon, with an intrinsic  $\gamma$ -ray sensitivity (limit of detection) estimated to approach  $\sim 0.02$ – $0.05$  photon. After exposure expires, resonance frequencies return to an ordinary tendency where the frequency variations are dominated by long-term drift. These  $\gamma$ -ray radiation induced frequency shifts are distinctive from those due to pressure variation or surface adsorption mechanisms. The measurements and analyses show that  $\text{MoS}_2$  resonators are robust yet sensitive to very low dosage  $\gamma$ -ray, demonstrating a potential for ultrasensitive detection and early alarm of radiation in the very low dosage regime. © 2016 AIP Publishing LLC.

[<http://dx.doi.org/10.1063/1.4939685>]

Radiations such as energetic subatomic particles or photons generated from nuclear reactions<sup>1</sup> have been exploited in a wide range of applications, from basic science (e.g., observing  $\gamma$ -ray bursts for studying cosmology<sup>2</sup>) to industry (e.g., electricity generation in nuclear plants) and nuclear medicine (e.g., imaging).<sup>3</sup> Meanwhile, with sufficient energy, such radiations may damage matters by breaking atomic bonds, ionizing atoms, or causing harmful biomolecular effects in living tissues.<sup>3</sup> To safely utilize radiations, it is desirable not only to develop various robust detectors capable of operating in harsh environments with high levels of radiations such as in nuclear reactors, but also to explore highly responsive and sensitive materials and devices for very early alarm of low dosage radiations or leakage. In all these scenarios, detection of ionizing radiations is of great importance for identifying, quantifying, and monitoring radiation sources and activities.

Historically gas-filled chambers have been the earliest for detecting ionizing radiations via the gas ionization. Since 1940s, scintillation crystals combined with photomultiplier tubes (PMT) have prevailed as the mainstream solutions in many applications to date. Later semiconductor junction devices have been extensively studied for compact pixel and array detectors.<sup>4,5</sup> Among the various possible semiconductor device platforms and detection mechanisms for ionizing radiations, resonant micro/nanoelectromechanical systems (MEMS/NEMS) offer excellent promises and sustainable improvement with device scaling.<sup>6,7</sup> In particular, because NEMS resonances are exceptionally responsive to variations in their modal masses and stiffnesses, considerable interests and efforts have been stimulated in exploiting

nanoresonators for ultrasensitive detection of physical quantities such as mass and force, attaining yocto-gram ( $10^{-24}$  g)<sup>8</sup> and zepto-newton ( $10^{-21}$  N)<sup>7</sup> sensitivities. Responses of nanoresonators to radiations such as  $\gamma$ -ray particles, however, have not yet been reported.

Atomic layer crystals, such as graphene and molybdenum disulfide ( $\text{MoS}_2$ ), have emerged as advanced materials for 2D electronic,<sup>9,10</sup> mechanical,<sup>11–15</sup> and optical<sup>16</sup> devices. Responses of graphene transistors to radiations have been recently investigated.<sup>17–19</sup> In contrast to graphene as a semimetal,<sup>20</sup>  $\text{MoS}_2$  is a semiconductor with bandgaps (BGs) near 1.3–1.9 eV, depending on its number of layers<sup>21</sup> and comparable with BGs of conventional semiconductor radiation detectors. Moreover,  $\text{MoS}_2$  possesses higher interaction probability (Eq. (1)) with  $\gamma$ -ray radiation than graphene does (given the same number of layers, down to monolayer limit), owing to its larger thickness per unit layer, and higher mass density (see Fig. 1(c)).

In this work, we explore effects of  $\gamma$ -ray radiation on multilayer  $\text{MoS}_2$  nanoresonators (Figs. 1(a) and 1(b)). We perform  $\gamma$ -ray irradiation using a 1mCi  $^{137}\text{Cs}$  source and monitor resonance responses of  $\text{MoS}_2$  nanoresonators to demonstrate the  $\gamma$ -ray radiation effects. We observe resonance upshifts in all devices upon irradiation, caused by ionizing  $\gamma$ -ray induced charging and charge-induced tensioning. Quantitative calculations with radiation dosage show that the  $\text{MoS}_2$  nanoresonators exhibit promise for sub-single  $\gamma$ -ray photon sensitivity.

$\text{MoS}_2$  drumhead nanoresonators are fabricated by mechanical exfoliation onto lithographically patterned 290 nm- $\text{SiO}_2$ -on-Si substrate with circular microtrenches,<sup>13</sup> with diameters  $d \approx 5$ – $6$   $\mu\text{m}$  and thicknesses from few-layer to thin film of  $t \approx 30$ – $80$  nm. After exfoliation,  $\text{MoS}_2$  resonators are annealed at 300 °C for 3 h in vacuum to remove surface

<sup>a)</sup>J. Lee and M. J. Krupcale contributed equally to this work.

<sup>b)</sup>Author to whom correspondence should be addressed. Electronic mail: philip.feng@case.edu

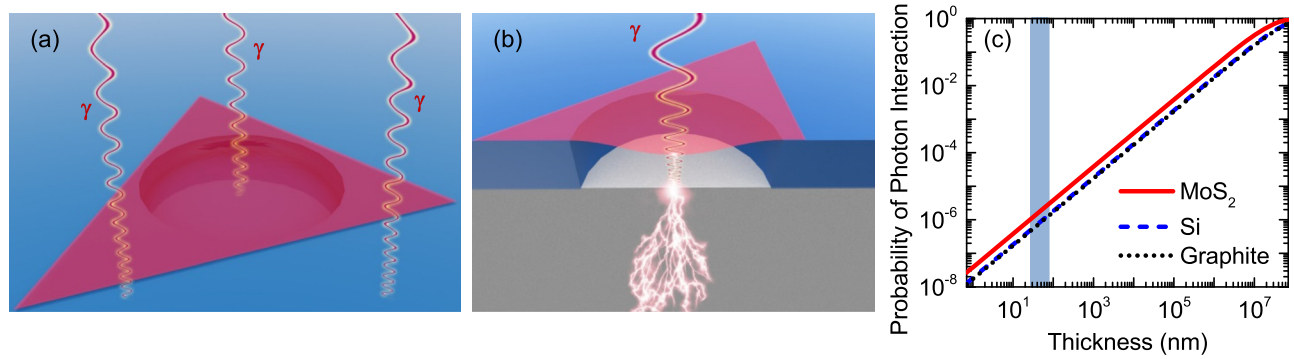


FIG. 1. Illustrations of  $\gamma$ -ray irradiation and calculated interaction probability of photons and a MoS<sub>2</sub> nanoresonator. (a) Aerial and (b) cross-sectional illustrations of  $\gamma$ -ray irradiation on a MoS<sub>2</sub> resonator, demonstrating generations of secondary  $\gamma$  photons and fast electrons. (c) Calculated interaction probability of 662 keV  $\gamma$ -ray on MoS<sub>2</sub> (red line) and Si (blue dashed line) and graphite (black dotted line). Blue colored regime indicates thickness of employed MoS<sub>2</sub> resonators.

adsorbates and restore the devices, and devices are promptly transferred into a vacuum chamber after annealing. Among fabricated resonators, we employ three completely sealed MoS<sub>2</sub> diaphragms and two partially covered drumheads with holes, which allow air flow in cavity.<sup>15</sup> All measurements, including  $\gamma$ -ray exposure and resonance, are performed in moderate vacuum ( $\sim 20$  mTorr) to eliminate measureable air damping.

We first estimate the interaction probability between a  $\gamma$ -ray photon and the MoS<sub>2</sub> resonator. The probability of monoenergetic photons traveling through a medium of thickness  $x$  without interaction is  $e^{-\mu x}$ , where  $\mu$  is the total linear attenuation coefficient mainly due to Compton scattering and photoelectric effect.<sup>4,5</sup> The interaction probability is

$$P = 1 - e^{-(\mu/\rho)\rho x}, \quad (1)$$

where  $\mu/\rho$  is total (Compton + photoelectric) mass attenuation coefficient per density, and  $\rho x$  the mass thickness of the absorber (MoS<sub>2</sub> here).<sup>5</sup> As MoS<sub>2</sub> is a compound, we have<sup>5</sup>

$$(\mu/\rho)_C = \sum w_i (\mu/\rho)_i, \quad (2)$$

where  $w_i$  is the weight fraction of element  $i$  (Mo, S). The calculated mass attenuation coefficients in MoS<sub>2</sub> using Eq. (2) are summarized in Table I. With Eq. (1) and results in Table I, the probability of a photon interacting with the MoS<sub>2</sub> drumhead is  $P_{\text{MoS}_2} \approx 1.5 - 3.1 \times 10^{-6}$ , depending on thickness of devices (see Fig. 1(c)). These calculations, however, neglect secondary  $\gamma$ -ray or fast electrons that may have been produced. Thus, the actual interaction rates with the MoS<sub>2</sub> nanoresonators can be larger than the calculated values. Consider the ultrathin MoS<sub>2</sub>, most of the  $\gamma$ -ray photons interact with the  $\sim 550 \mu\text{m}$ -thick Si substrate (underneath the vibrating MoS<sub>2</sub> resonators and the  $\sim 290 \text{ nm}$  SiO<sub>2</sub>).

We then calibrate the incident photon flux on device to quantify radiation exposure. The  $\gamma$ -ray dosage is measured using a calibrated NaI scintillator. The radiation flux on the circular cylindrical detector is

$$\dot{\Phi} = \frac{N_p(L, E)}{S_D t_L \varepsilon_i(E)}, \quad (3)$$

where  $E$  is energy of  $\gamma$ -ray,  $S_D$  the scintillator detector's effective surface area,  $N_p$  the number of events recorded in the photopeak,  $t_L$  the exposure time, and  $L$  the distance from source to detector. Since the intrinsic peak efficiency  $\varepsilon_i(E)$  is unknown and depends on detector material, radiation energy, and detector thickness, we first calibrate the employed NaI detector. Detector peak efficiency can be separated into two components,  $\varepsilon_p(L, E) = \varepsilon_G(L) \varepsilon_i(E)$ , where  $\varepsilon_G(L)$  is the geometrical efficiency. In the case of an isotropic point source, geometrical efficiency is  $\varepsilon_G(L) = \Omega(L)/4\pi$ . Here,  $\Omega(L)$  is the solid angle of the detector relative to the source position. If the source is located along the axis of a circular cylinder detector of radius  $r$ , we have  $\Omega(L) = 2\pi[1 - L(L^2 + r^2)^{-1/2}]$ .<sup>5</sup> The absolute source activity is  $A = N_p(L, E)/[t_L \varepsilon_p(L, E) I_\gamma(E)]$ , where  $I_\gamma(662 \text{ keV}) \approx 0.85$  is the photon emission probability. The detector peak efficiency for such geometry can be rewritten as

$$\varepsilon_p(L, E) = \frac{N_p(L, E)}{A t_L I_\gamma(E)} = \frac{\varepsilon_i(E)}{2} \left(1 - \frac{L}{\sqrt{L^2 + r^2}}\right). \quad (4)$$

The source activity  $A = A_0(1/2)^{t/T_{1/2}}$  can be estimated at a particular time  $t$  if its initial activity  $A_0$  is known, where  $T_{1/2}$  is the isotope half-life time. For 662 keV <sup>137</sup>Cs,  $T_{1/2} = 10986 \pm 33$  days. By using a radiation source with a given activity and the photopeak counts, the detector photopeak efficiency,  $\varepsilon_p(L, E)$ , can be plotted against the source-detector distance (Figs. 2(a) and 2(b)). From the fitting, we obtain intrinsic peak efficiency of  $\varepsilon_i(E) \approx 0.099$  at 662 keV (Fig. 2(c)) from  $\sim 1 \text{ mCi}$  <sup>137</sup>Cs source. We thus estimate that the flux 5 cm away from the source is  $\dot{\Phi} \approx 2.4 \times 10^9 \text{ photon/m}^2\text{s}$ .

After the careful calibration of dosage, we focus on measuring MoS<sub>2</sub> resonance responses before and after radiation exposure. Immediately after annealing at 300 °C for 3 h in vacuum, thermomechanical resonances of MoS<sub>2</sub> devices are

TABLE I. Photon mass attenuation coefficients ( $\mu/\rho$ ) of MoS<sub>2</sub> due to different interaction mechanisms. The unit for the mass attenuation coefficients is [ $\text{cm}^2 \text{g}^{-1}$ ].

$E_\gamma$ (keV)	Scattering			Pair production		Total attenuation	
	Coherent (Rayleigh)	Incoherent (Compton)	Photoelectric absorption	Nuclear field	Electron field	With Rayleigh	Without Rayleigh
662	$1.492 \times 10^{-3}$	$7.103 \times 10^{-2}$	$2.851 \times 10^{-3}$	0	0	$7.537 \times 10^{-2}$	$7.388 \times 10^{-2}$

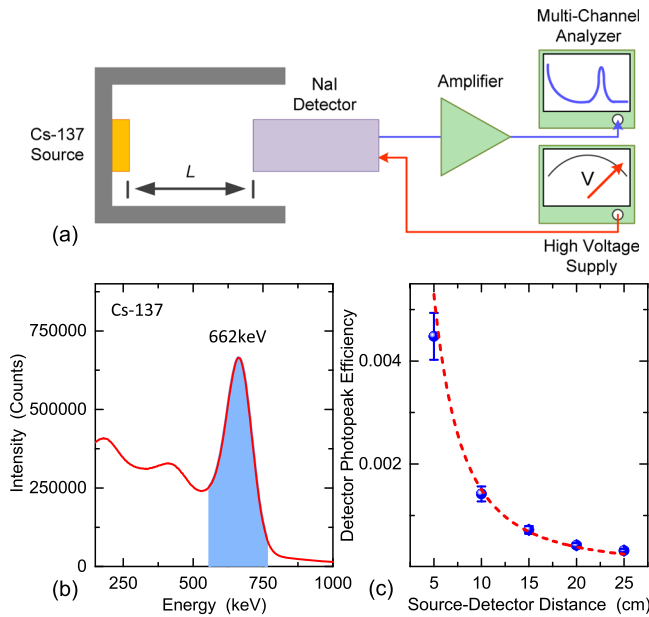


FIG. 2. Intrinsic peak efficiency of the NaI detector. (a) Schematic of measurement configuration for calibrating the NaI detector. (b) Measured photopeak from  $^{137}\text{Cs}$  source using the NaI scintillation detector. (c) Measured detector photopeak efficiency,  $\varepsilon_p(L, E)$ , with varying source-to-detector distance. Red dashed line shows fitting results using Eq. (3) and estimated intrinsic peak efficiency of the NaI detector is  $\varepsilon_i(E) \approx 9.9\%$ .

monitored without  $\gamma$ -ray exposure using a customized optical interferometry system sketched in Fig. 3(c).<sup>12,22</sup> As shown in Figs. 4 and 5, resonances of the devices are in the range of  $\sim 15$ – $21$  MHz and gradually drift toward lower frequency over long time. This drift is attributed to slow adsorption of air molecules onto devices (inside moderate vacuum). After tracking resonances over 36 h (Figs. 5(a)–5(d)), we locate the  $\sim 1\text{mCi}$   $^{137}\text{Cs}$  sealed source  $\sim 5$  cm away from the resonators, and expose the devices to 662 keV  $\gamma$ -ray radiation for  $\sim 24$  h in vacuum (Fig. 3). During the radiation exposure period,

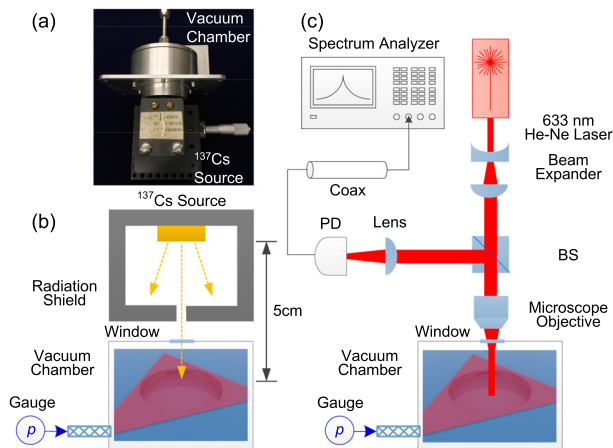


FIG. 3. Experimental system for radiation exposure and optical interferometric resonance readout. (a) Photograph of the vacuum chamber and the  $^{137}\text{Cs}$  radiation source. (b) Illustration of the radiation exposure scheme.  $\text{MoS}_2$  resonators are located in a vacuum chamber and exposed to  $\gamma$ -ray photons through an optical window. The distance from  $^{137}\text{Cs}$  source to resonators is  $L \approx 5$  cm. (c) Schematic of a customized optical interferometry setup. A 633 nm HeNe laser is focused onto devices, and Brownian motions of resonators are monitored. All measurements are carried out in moderate vacuum and at room temperature.

each device is exposed to  $N_{\text{total}} \approx 5000$   $\gamma$ -ray photons at 662 keV, estimated from radiation flux upon given device area and exposure time. The number of photons interacting with  $\text{MoS}_2$  devices is  $N_{\text{MoS}_2} = N_{\text{total}} \times P_{\text{MoS}_2} \approx 0.01$  photon, suggesting that thin  $\text{MoS}_2$  nanoresonators are mostly transparent for high energy  $\gamma$ -ray photons. After 24 h of exposure, the  $^{137}\text{Cs}$  source is removed, and the resonances are monitored again for  $\sim 60$  h. Immediately after  $\gamma$ -ray exposure, all the resonators exhibit  $\sim 0.5$ – $2.1\%$  resonance frequency upshifts, which correspond to radiation responsivity ( $\mathfrak{R} = \Delta f/N_{\text{total}}$ ) of  $\mathfrak{R} \approx 30$  to 82 Hz/photon. After that, resonances of all the devices return to their initial tendency of ordinary long-term drifting. Once resonances return to the drifting trend, they do not exhibit further noticeable frequency upshifts. For Device #5, we apply a shorter period (12 h) of  $\gamma$ -ray exposure, while measuring the resonance with much shorter intervals before and after exposure. The data in Fig. 5(e) clearly demonstrate the same signature of repeatable and robust frequency upshift.

Further, we estimate the intrinsic  $\gamma$ -ray radiation resonant sensitivity (limit of detection) of a  $\text{MoS}_2$  nanoresonator by employing its intrinsic frequency stability. Frequency stability given by fractional frequency fluctuations over averaging time  $\tau$  is<sup>23</sup>

$$\left\langle \frac{\Delta f_0}{f_0} \right\rangle_{\tau} = \left( \frac{1}{Q} \right) \times \left( \frac{\pi k_B T}{P_c \tau} \right)^{1/2}, \quad (5)$$

where  $f_0$  is resonance frequency,  $Q$  is quality factor,  $k_B$  is Boltzmann constant,  $T$  is temperature, and  $\tau$  is averaging time. Here,  $P_c = \pi f_0 k_{\text{eff}} a_c^2 / Q$  is operating power of the resonator,  $k_{\text{eff}}$  is effective stiffness, and  $a_c$  is displacement at critical point.<sup>24</sup> For Device #1, the measured critical point response gives  $a_c \approx 1.5$  nm, which yields  $P_c \approx 3$  pW. At  $T \approx 300$  K, estimated frequency stability of Device #1 with 1 s averaging time ( $\tau = 1$  s) is  $\langle \delta f_0 / f_0 \rangle_{\tau=1\text{s}} = 1.1 \times 10^{-7}$ , and thus  $\delta f_0 \approx 2$  Hz. This stability level leads to a  $\gamma$ -ray radiation sensitivity of  $\delta f_0 / \mathfrak{R} \approx 0.02$ – $0.05$  photon for Devices #1–#5 ( $\tau = 1$  s), showing deep sub-single  $\gamma$ -ray photon limit of detection. If we relax the frequency stability to a modest  $2 \times 10^{-6}$ , compromised by extrinsic noise and practically more achievable,<sup>8,23</sup> this leads to  $\gamma$ -ray photon sensitivity of  $\sim 0.5$ – $1$  photon (for Devices #1–#5).

The observed resonance upshifts (in all devices) upon radiation exposure can be understood by examining charge generation in the device structure. Among reasons that may vary resonances, we can first exclude adsorption-induced frequency shifts where downshifts are expected due to added mass. In addition, we can also rule out frequency shifts associated with membrane bulging due to pressure change in sealed cavity, because devices with both sealed and leaking cavities exhibit the same frequency upshifts upon radiation. Hence, the most relevant mechanism of radiation effects on these resonators is generation and interaction of charges. Because we carefully anneal each device before any measurement (an established protocol for restoring the device), without radiation exposure, resonance frequency slowly drifts toward lower frequency, due to adsorption of air molecules over time (Fig. 6).

During radiation exposure, the direct interaction probabilities of a  $\gamma$ -ray photon with the  $\text{MoS}_2$  resonators are very

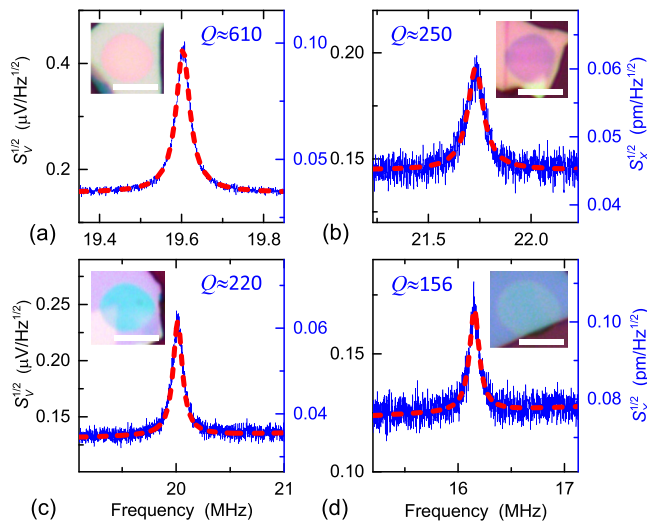


FIG. 4. Measured undriven thermomechanical resonances from MoS<sub>2</sub> drum-head resonators. (a)–(d) Measured resonances immediately after annealing from Device #1 ( $d \approx 5.4 \mu\text{m}$ ,  $t \approx 31 \text{ nm}$ ), Device #2 ( $d \approx 5.5 \mu\text{m}$ ,  $t \approx 51 \text{ nm}$ ), Device #3 ( $d \approx 5.6 \mu\text{m}$ ,  $t \approx 55 \text{ nm}$ ), and Device #4 ( $d \approx 6.1 \mu\text{m}$ ,  $t \approx 81 \text{ nm}$ ), respectively. Device #4 has a small opening, which acts as a leaking aperture. Red dashed lines show fitting results using a finite- $Q$  harmonic resonator model. Insets show optical images of devices. All scale bars are  $5 \mu\text{m}$ .

small,  $P_{\text{MoS}_2} \approx 1.5 - 3.1 \times 10^{-6}$  (from Eqs. (1) and (2), Fig. 1(c)), because of the very thin devices, thus most  $\gamma$ -ray photons first strike the much thicker SiO<sub>2</sub>/Si substrate underneath the vibrating MoS<sub>2</sub>, producing secondary  $\gamma$ -ray photons and fast electrons, which interact with the device structure again and further create larger numbers of  $\gamma$  photons and secondary electrons (SE) (Fig. 6(c)). These cascade multi-interactions generate trapped charges in the device

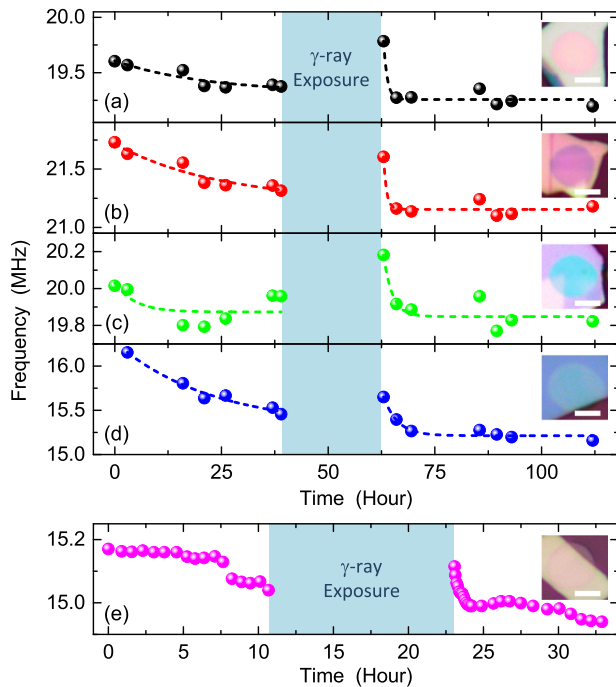


FIG. 5. Measured resonance frequencies versus time before and after  $\gamma$ -ray radiation exposure. (a)–(d) Measured frequency evolution from Device #1, Device #2, Device #3, and Device #4, respectively. Each of the resonators is exposed for  $\sim 24 \text{ h}$  (light blue region). (e) Data from Device #5 with  $\sim 12 \text{ h}$  of exposure and much shorter measurement intervals. Insets show optical images of the individual MoS<sub>2</sub> resonators. All scale bars are  $3 \mu\text{m}$ .

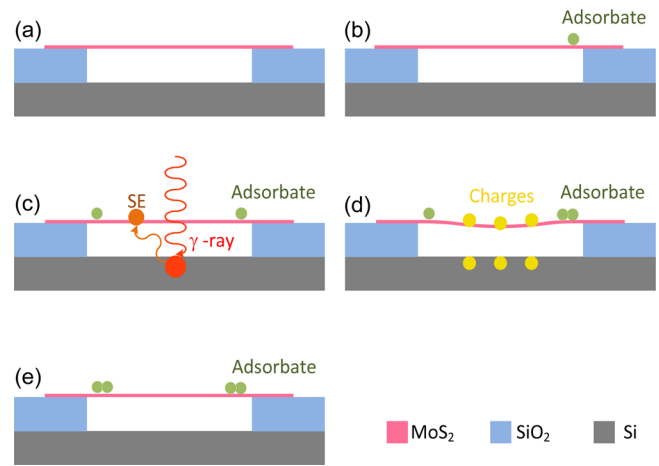


FIG. 6. Illustrations of  $\gamma$ -ray radiation effects on a MoS<sub>2</sub> resonator. (a) Clean MoS<sub>2</sub> resonator right after annealing. (b) Air molecules adsorbing on device surface. (c)  $\gamma$ -ray irradiation onto device, generating secondary  $\gamma$ -ray photons and fast electrons. (d)  $\gamma$ -ray irradiation described in (c) produces trapped charges, which causes electrostatic forces, tension, and deformation of the MoS<sub>2</sub> resonator. (e) Generated trapped charges are neutralized over time after radiation expires.

structure across the SiO<sub>2</sub> layer (Figs. 6(c) and 6(d)) and cause electrostatic forces between the charged MoS<sub>2</sub> drum-head and the Si substrate, resulting in electrostatic tension and deflection of the MoS<sub>2</sub> drumheads (Fig. 6(d)), and the resonance frequency upshifts. After exposure expires, trapped charges are neutralized over time, so that the resonance frequencies return to the initial frequency tendency (Fig. 6(e)). We note that the quantitative details of the charging mechanism of  $\gamma$ -ray interaction with the device structure may depend on the work function of the Si substrate. It could be interesting to alter and engineer the work function of the substrate by depositing different metals of interest, or forming metal silicides on the Si substrate, and investigate how the device resonance changes with the work function.

Furthermore, we estimate the tension and deflection induced in MoS<sub>2</sub>, based on the measured frequency upshifts. The resonance frequency of clamped circular drumhead resonators in this study can be determined by<sup>25,26</sup>

$$f_0 = \frac{1}{2\pi} \left( k \frac{d}{2} \right) \left( \frac{16D}{\rho t d^4} \left[ \left( k \frac{d}{2} \right)^2 + \frac{\sigma t d^2}{4D} \right] \right)^{1/2}, \quad (6)$$

where  $d$  is the diameter,  $t$  the thickness,  $D = E_Y t^3 / [12(1 - \nu^2)]$  the bending rigidity,  $\sigma$  the tension [N/m<sup>2</sup>],  $E_Y$  the Young's modulus,  $\rho$  the density, and  $\nu$  the Poisson's ratio of MoS<sub>2</sub>, and  $k$  is the mode parameter determined numerically.<sup>26</sup> Extracted Young's modulus of MoS<sub>2</sub> from the resonances data is 0.2–0.4 TPa, showing good agreement with the previously reported values.<sup>13,27</sup> For further analysis, we employ Device #1 which particularly does not consist of structural defects (e.g., thickness variation or holes) for modeling. The initial surface tension on MoS<sub>2</sub> resonators is  $\sim 0.1 \text{ N/m}$  (6.84 ppm of strain).<sup>13</sup> Upon  $\gamma$ -ray exposure, the resonance frequency of Device #1 shifts from  $\sim 19.375 \text{ MHz}$  to  $\sim 19.784 \text{ MHz}$ , which yields a tension level of  $\sim 0.240 \text{ N/m}$  (16.41 ppm of strain), corresponding to  $\sim 12 \text{ nm}$  static displacement at the center of the diaphragm.

In conclusion, we have examined 662 keV  $\gamma$ -ray radiation effects from 1mCi  $^{137}\text{Cs}$  source upon 2D  $\text{MoS}_2$  nanomechanical resonators. Our results show that  $\text{MoS}_2$  nanoresonators offer excellent  $\gamma$ -ray radiation sensitivity, which would be particularly relevant in environments where radiation dosage is very low and early detection and alarm are desired. In addition, their small device footprints promise integration of  $\text{MoS}_2$  resonators on chip, suggesting the possibilities for enabling compact and portable radiation detectors.

We thank the support from the Case School of Engineering, National Academy of Engineering (NAE) Grainger Foundation Frontier of Engineering (FOE) Award (FOE2013-005), National Science Foundation CAREER Award (ECCS #1454570), and DTRA Basic Scientific Research Program (Grant No. HDTRA1-15-1-0039). We thank Professor Michael Martens from Department of Physics for his generous support.

<sup>1</sup>E. Segrè, *Nuclei and Particles*, 2nd ed. (Addison-Wesley Pub. Co. Inc., Redwood City, CA, 1982).

<sup>2</sup>N. Gehrels and P. Mészáros, *Science* **337**, 932–936 (2012).

<sup>3</sup>S. R. Cherry, J. A. Sorenson, and M. E. Phelps, *Physics in Nuclear Medicine*, 4th ed. (Elsevier Saunders, Philadelphia, PA, 2012).

<sup>4</sup>C. F. G. Delaney and E. C. Finch, *Radiation Detectors: Physical Principles and Applications* (Clarendon Press, Oxford, UK, 1992).

<sup>5</sup>G. F. Knoll, *Radiation Detection and Measurement*, 4th ed. (John Wiley & Sons, New York, 2010).

<sup>6</sup>Y. T. Yang, C. Callegari, X. L. Feng, K. L. Ekinci, and M. L. Roukes, *Nano Lett.* **6**, 583–586 (2006).

<sup>7</sup>J. Moser, J. Güttinger, A. Eichler, M. J. Esplandiu, D. E. Liu, M. I. Dykman, and A. Bachtold, *Nat. Nanotechnol.* **8**, 493–496 (2013).

<sup>8</sup>J. Chaste, A. Eichler, J. Moser, G. Ceballos, R. Rurali, and A. Bachtold, *Nat. Nanotechnol.* **7**, 301–304 (2012).

<sup>9</sup>F. Schwierz, *Nat. Nanotechnol.* **5**, 487–496 (2010).

<sup>10</sup>B. Radisavljevic, A. Radenovic, J. Brivio, V. Giacometti, and A. Kis, *Nat. Nanotechnol.* **6**, 147–150 (2011).

<sup>11</sup>J. S. Bunch, A. M. van der Zande, S. S. Verbridge, I. W. Frank, D. M. Tanenbaum, J. M. Parpia, H. G. Craighead, and P. L. McEuen, *Science* **315**, 490–493 (2007).

<sup>12</sup>C. Chen, S. Lee, V. V. Deshpande, G.-H. Lee, M. Lekas, K. Shepard, and J. Hone, *Nat. Nanotechnol.* **8**, 923–927 (2013).

<sup>13</sup>J. Lee, Z. Wang, K. He, J. Shan, and P. X.-L. Feng, *ACS Nano* **7**, 6086–6091 (2013).

<sup>14</sup>J. Lee and P. X.-L. Feng, in *Proceedings of IEEE International Frequency Control Symposium (IFCS), Taipei, Taiwan, 19–22 May 2014*, pp. 282–285.

<sup>15</sup>J. Lee, Z. Wang, K. He, J. Shan, and P. X.-L. Feng, *Appl. Phys. Lett.* **105**, 023104 (2014).

<sup>16</sup>A. N. Grigorenko, M. Polini, and K. S. Novoselov, *Nat. Photonics* **6**, 749–758 (2012).

<sup>17</sup>I. Childres, L. A. Jauregui, M. Foxe, J. Tian, R. Jalilian, I. Jovanovic, and Y. P. Chen, *Appl. Phys. Lett.* **97**, 173109 (2010).

<sup>18</sup>M. Foxe, G. Lopez, I. Childres, R. Jalilian, A. Patil, C. Roecker, J. Boguski, I. Jovanovic, and Y. P. Chen, *IEEE Trans. Nanotechnol.* **11**, 581–587 (2012).

<sup>19</sup>O. Koybasi, I. Childres, I. Jovanovic, and Y. P. Chen, *Proc. SPIE* **8373**, 83730H (2012).

<sup>20</sup>A. K. Geim, *Rev. Mod. Phys.* **83**, 851 (2011).

<sup>21</sup>K. F. Mak, C. Lee, J. Hone, J. Shan, and T. F. Heinz, *Phys. Rev. Lett.* **105**, 136805 (2010).

<sup>22</sup>Z. Wang, J. Lee, and P. X.-L. Feng, *Nat. Commun.* **5**, 5158 (2014).

<sup>23</sup>X. L. Feng, C. J. White, A. Hajimiri, and M. L. Roukes, *Nat. Nanotechnol.* **3**, 342–346 (2008).

<sup>24</sup>Z. Wang and P. X.-L. Feng, *Appl. Phys. Lett.* **104**, 103109 (2014).

<sup>25</sup>T. Wah, *J. Acoust. Soc. Am.* **34**, 275–281 (1962).

<sup>26</sup>H. Suzuki, N. Yamaguchi, and H. Izumi, *Acoust. Sci. Technol.* **30**, 348–354 (2009).

<sup>27</sup>S. Bertolazzi, J. Brivio, and A. Kis, *ACS Nano* **5**, 9703–9709 (2011).